nanomaterials

MDPI

Article

Cobalt–Graphene Catalyst for Selective Hydrodeoxygenation of Guaiacol to Cyclohexanol

Qichang Guo, Jingbo Mao, Shenmin Li, Jingmei Yin, Yang Lv and Jinxia Zhou *

College of Environmental and Chemical Engineering, Dalian University, Dalian 116622, China
* Correspondence: zhoujinxia@dlu.edu.cn; Tel.: +86-411-87403214; Fax: +86-411-87402449

Abstract: Herein, cobalt-reduced graphene oxide (rGO) catalyst was synthesized with a practical impregnation–calcination approach for the selective hydrodeoxygenation (HDO) of guaiacol to cyclohexanol. The synthesized Co/rGO was characterized by transmission electron microscopy (TEM), high-angle annular dark-field scanning TEM (HAADF-STEM), X-ray photoelectron spectroscopy (XPS), Raman spectroscopy, X-ray diffraction (XRD), and H_2 temperature-programmed reduction (H_2-TPR) analysis. According to the comprehensive characterization results, the catalyst contains single Co atoms in the graphene matrix and Co oxide nanoparticles (CoO_x) on the graphene surface. The isolated Co atoms embedded in the rGO matrix form stable metal carbides (CoC_x), which constitute catalytically active sites for hydrogenation. The rGO material with proper amounts of N heteroatoms and lattice defects becomes a suitable graphene material for fabricating the catalyst. The Co/rGO catalyst without prereduction treatment leads to the complete conversion of guaiacol with 93.2% selectivity to cyclohexanol under mild conditions. The remarkable HDO capability of the Co/rGO catalyst is attributed to the unique metal–acid synergy between the CoC_x sites and the acid sites of the CoO_x nanoparticles. The CoC_x sites provide H while the acid sites of CoO_x nanoparticles bind the C-O group of reactants to the surface, allowing easier C-O scission. The reaction pathways were characterized based on the observed reaction–product distributions. The effects of the process parameters on catalyst preparation and the HDO reaction, as well as the reusability of the catalyst, were systematically investigated.

Keywords: cobalt–graphene catalyst; Co single atoms; Co oxide nanoparticles; hydrodeoxygenation; guaiacol; cyclohexanol

Citation: Guo, Q.; Mao, J.; Li, S.; Yin, J.; Lv, Y.; Zhou, J. Cobalt–Graphene Catalyst for Selective Hydrodeoxygenation of Guaiacol to Cyclohexanol. *Nanomaterials* **2022**, *12*, 3388. https://doi.org/10.3390/nano12193388

Academic Editor: Sónia Carabineiro

Received: 31 August 2022
Accepted: 24 September 2022
Published: 28 September 2022

1. Introduction

The excessive consumption of fossil resources results in diminishing petroleum supply and severe environmental pollution. As a renewable energy resource, abundant and carbon-neutral biomass has been extensively explored for the production of highly valuable chemicals and biofuels [1]. However, the production of biomass-derived compounds with good selectivity remains challenging because of the complex structures and diverse oxygenic groups in biomass-derived feedstock [2]. Currently, catalytic hydrodeoxygenation (HDO) is considered the most efficient approach for upgrading biomass derivatives, and the development of cost-effective catalysts is key to this process [3]. As a main component of biomass, lignin is a planted polymer composed of phenylpropanoid building units that potentially provide renewable six-ring compounds [4]. Given the complex structure of lignin, guaiacol (GUA; 2-methoxyphenol), which contains two common oxygenate groups in lignin: methoxy (C_{aryl}–OCH_3) and phenolic (C_{aryl}–OH) groups, is extensively used as a lignin model compound in catalytic studies of lignin derivatives [5].

HDO of GUA involves combinations of different reactions such as hydrogenation, hydrogenolysis, and dehydration. Different elementary reactions usually occur at different catalytic sites. Typically, the heterogeneous catalysts designed for HDO contain two functions: one is for hydrogen dissociation, while the other is for the C-O activation [6]. To date,

a wide range of metal catalysts has been studied for the HDO of GUA. Selective removal of the methoxy group and hydrogenation saturation of the aromatic ring of GUA can produce cyclohexanol (CYHAOL), an important feedstock in the chemical industry [7]. However, the production of CYHAOL from GUA is challenging because versatile hydrogenation processes generate various products. For instance, excessive HDO of GUA forms cyclohexane (CYHA) over numerous catalysts [2,8–12]. Table S1 lists the catalysts identified for the selective HDO of GUA to CYHAOL reported in recent years. Various noble metal catalysts, such as Ru [13] and bimetallic catalysts composed of Ru–Re [14], Ru–Mo [15], Ru–Co [16], and Au–Rh [17], have been widely investigated for the HDO of GUA to CYHAOL. On the other hand, some studies have focused on the development of low-cost transition metal catalysts. Some Ni-based catalysts [18–25] and Co-based catalysts [26–28] catalyzed HDO of GUA with CYHAOL as the main product. In particular, the production of CYHAOL in more than 90% yield was achieved over several Co-containing catalysts, including Ru–Co supported on active carbon [16], Ni–Co supported carbon nanotubes [25], and Co supported on TiO_2 [27]. In this study, we worked to develop a new Co-based catalyst for HDO of GUA with high selectivity to CYHAOL.

Table S2 lists Co-based catalysts used in HDO of GUA. In addition to forming CYHAOL [26–28], some Co-based catalysts lead to CYHA [8,9], phenol (Ph) [29,30] and benzene [31,32] products. As shown in Table S2, the Co-based catalysts were reduced with H_2 [8,9,26,27,29,30,32], NH_3 [28], or in situ co-pyrolysis with cellulose [31] before use, indicating the reduction treatment of the catalysts was necessary for catalytic activity. For instance, the Co/TiO_2 catalyst without reduction by H_2 generated no propylcyclohexanol production in selective HDO of eugenol [27]. When reduced in H_2 flow at 600 °C for 2 h, it showed excellent HDO activity, achieving >99.9% propylcyclohexanol yield under 1 MPa H_2, 200 °C for 2 h [27]. Magnetic CoN_x@NC catalysts synthesized by co-pyrolysis of cellulose and $Co(NO_3)_2$ under an ammonia atmosphere at 650 °C also exhibited good HDO activity for eugenol conversion to propylcyclohexanol [28]. It was noted that the excellent catalytic activity of CoN_x@NC-650 for propylcyclohexanol formation was mainly ascribed to the CoN_x species rather than metallic Co (Co^0). In addition to transition metals and metal nitrides, carbides are alternative catalytic hydrogenation materials [33]. Metal carbides, such as Co carbide [34], exhibit specific catalytic hydrogenation features in Fischer−Tropsch to olefins reaction. Conventional carbides are a class of interstitial compounds with carbon atoms filled in the crystal structure of the metals. When the metals lose the crystal structures due to excessive dispersion of the metals to nanoparticles, clusters, and even single atoms, the formation of stable metal carbides occurs on carbon composites in crystal structures. In this case, graphene offers many benefits as a carbon support [35]. Graphene is a good support for embedding single metal atoms in the graphene matrix [36]. In addition, the high surface area of graphene promotes the dispersion of active phases, and graphene with good electrical conductivity may be used to modulate the electronic properties of the metal-active sites, thus governing their HDO performance [37].

In this study, the selective HDO of GUA to CYHAOL was investigated over graphene-supported Co catalysts synthesized using a concise and scalable approach. Initial catalyst screening studies demonstrated that Co/reduced graphene oxide (rGO) catalysts are highly suitable for the HDO of GUA to CYHAOL. The structure and composition of the Co/rGO catalyst were characterized through transmission electron microscopy (TEM), high-angle annular dark-field scanning TEM (HAADF-STEM), X-ray photoelectron spectroscopy (XPS), Raman spectroscopy, X-ray diffraction (XRD), and H_2 temperature-programmed reduction (H_2-TPR) analysis. The characterization and catalytic experiments revealed the unique catalytic functions of single Co atoms embedded in the graphene matrix and Co oxide nanoparticles on the graphene surface. The effects of heteroatoms in graphene and the conditions of catalyst preparation and reaction, as well as the reusability of the catalyst, were also investigated in detail.

2. Materials and Methods

2.1. Synthesis of Co-Based Catalysts

rGO was prepared according to a previously reported method [38]. The reduction of graphene oxide (GO) with hydrazine hydrate generated rGO, and GO was prepared with a modified Hummers' method [38,39]. N-free reduced graphene oxide (rGO*) was prepared by reducing GO with sodium borohydride at 80 °C [40]. Commercial graphene (Gr) was supplied by Aladdin Chemical Reagent Co., Ltd. (China). Cobalt nitrade, ferric nitrade, and nickel nitrade were used to provide the transition metal components of Co, Ni, and Fe, respectively. Comparison experiments were conducted using γ-Al_2O_3 (Shandong Filiale of China Aluminum Co., Ltd., Zibo, China; calcined at 500 °C in air before use) and HY zeolite (SAR = 2.6; Wenzhou Huahua Co., Ltd., Wenzhou, China) as supports. The catalysts were prepared with the impregnation–calcination method. The metal loadings were quantitatively confirmed by incipient-wetness impregnation. The typical operations were as follows: First, a cobalt nitrate solution was prepared with an ethanol–water mixture (volume ratio, 1:4); second, Co was dispersed on the support surface with the incipient–wetness impregnation method; the impregnation mixture was vacuum-dried at 50 °C for 12 h; finally, the dried sample was calcined at 500 °C under N_2 flow in a tube furnace for 2 h (heating rate, 10 °C/min). The prepared catalysts were designated as Co_x/support, where x represents the amount of Co metal loaded per gram of support (mmol/g). The catalysts were used in the reactions without prereduction treatment. CoO_x powder was synthesized for mechanism study through a precipitation method: a cobalt nitrate solution was precipitated with a 0.2 M NaOH solution, and the precipitate was calcined in air at 400 °C.

2.2. Characterization

Characterization methods included TEM, HAADF-STEM, XPS, XRD, Raman spectroscopy, low-temperature N_2 adsorption–desorption, CHNSO elemental analysis, thermogravimetric analysis (TGA), H_2-TPR, and NH_3 temperature-programmed desorption (NH_3-TPD) analysis. Detailed information regarding these methods is provided in the Supplementary Materials.

2.3. Catalytic HDO Tests

The HDO of the GUA reactions was conducted in an autocontrol reactor (50 mL; Beijing Century Senlang Experimental Apparatus Co. Ltd., Beijing, China). In a typical run, the reactor was loaded with guaiacol (300 mg), the catalyst (30 mg; without prereduction treatment) and n-dodecane (10 mL), and then pressurized with H_2 to 1 MPa at room temperature. The reactor was heated to the target temperature and allowed to operate for a specific time. The liquid products were mixed and diluted by ethanol, and then analyzed using an Agilent GC7820 gas chromatograph equipped with a flame ionization detector and SE-30 capillary column (Dalian Zhonghuida Scientific Instrument Co., Ltd., Dalian, China). n-Tetradecane was used as the internal standard. Recycle test of the catalyst was carried out as follows: after the reaction, the catalyst was recovered from the reaction mixture by centrifugal separation, washed with ethanol, and vacuum-dried without calcination for the subsequent run. The results were quantified as GUA conversion, product selectivity, and yield in molar percentage, based on the number of C6 rings in the substrate and products. The overall carbon balance of the products was in the range of experimental error (±3%). The guaiacol conversion (X_{GUA}), the Product i selectivity (S_i), and Product i yield (Y_i) were calculated as following Equations (1)–(3):

$$X_{GUA}(\text{mol\%}) = \frac{(\text{Moles of GUA})_{in} - (\text{Moles of GUA})_{out}}{(\text{Moles of GUA})_{in}} \times 100\% \quad (1)$$

$$S_i(\text{mol\%}) = \frac{\text{Moles of Product}_i}{(\text{Moles of GUA})_{in} - (\text{Moles of GUA})_{out}} \times 100\% \quad (2)$$

$$Y_i(\text{mol}\%) = \frac{\text{Moles of Product}_i}{(\text{Moles of GUA})_{in}} \times 100\% \quad (3)$$

3. Results and Discussion

3.1. Characterization

3.1.1. Electron Microscope Images

The morphology of the $Co_{2.5}$/rGO catalyst was characterized by TEM, HRTEM, and HAADF-STEM (Figure 1). The catalyst shows a homogenous dispersion of nanoparticles (Figure 1a) with an average size of 6.7 nm in the TEM image (Figure 1c). The HRTEM image (Figure 1b) exhibits the typical crystalline morphology of the nanoparticles. The lattice fringes close to 0.213 and 0.244 nm are ascribed to the CoO (200; JCPDS card: 65-2902) and Co_3O_4 (311) (JCPDS card: 43-1003) planes, respectively. The lattice fringes of metallic Co were not observed in the HRTEM images. The results indicate the co-existence of various Co oxides in the nanoparticles, which are termed as CoO_x. Single Co atoms embedded in the graphene sheet were confirmed by HAADF-STEM images (Figure 1d,e). The area marked with a circle is an example of a single Co atom. Figure 1e shows the homogeneous distribution and high density of isolated Co atoms in the graphene nanosheet. The prepared catalyst was calcined at 500 °C in N_2, and thus, the reserved Co single metal atoms were not physically adsorbed on the graphene sheet; by contrast, they built strong chemical bonding configurations with the rGO sheet. rGO is derived from GO through reduction treatments. After the removal of the oxygenic groups, the sp^3-hybridized C atoms were terminated with H bonds, forming lattice defects on the graphene plane. Chemical bonding of the isolated metal atoms with pristine intact graphene is not easy due to the high chemical stability of the graphene's honeycomb structure [41]. As confirmed theoretically and experimentally [41,42], the introduction of defective sites in the graphene matrix offers multifarious bonding configurations to guarantee the structural stability of metal atoms. The high density and homogeneous distribution of single Co metal atoms in the rGO sheet (Figure 1e) correspond to the high density and homogeneous distribution of lattice defects in the rGO structure. We named the Co single metal atoms in the graphene matrix as CoC_x sites, which are similar to metal carbides.

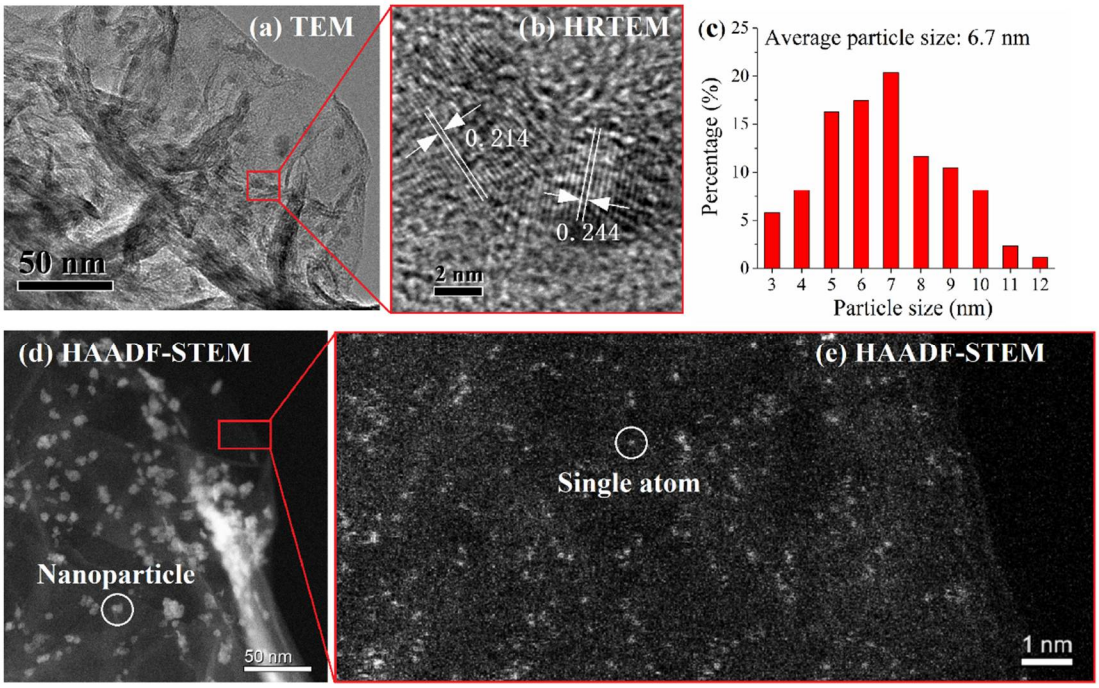

Figure 1. Characteristic results of $Co_{2.5}$/rGO including (**a**) TEM image, (**b**) HRTEM image, (**c**) particle size distribution, and (**d**,**e**) HAADF-STEM images.

3.1.2. XPS

The XPS results in Figure 2 provide information on the surface elemental constituents and valence state of the $Co_{2.5}$/rGO catalyst. Full-scan XPS survey spectrum (Figure S1 in the Supplementary Materials) shows the predominant presence of C, O, N, and Co elements. The Co^{2+} is characterized by the Co $2p_{3/2}$ peak at 782.1 eV, Co $2p_{1/2}$ peak at 798.0 eV, and corresponding shake-up resonances at approximately 787.9 and 803.6 eV [43]. The prominent peaks around 780.3 and 795.3 eV are assigned to the Co $2p_{3/2}$ and Co $2p_{1/2}$ peaks of the Co^{3+} configuration with an energy difference of 15 eV [43]. The Co 2p peaks of the bulk cobalt carbide (Co_2C) appear at 778.4 and 793.4 eV, which are at the binding energy in metallic Co [44]. In the $Co_{2.5}$/rGO catalyst, the Co single-atoms doped in the graphene matrix of rGO formed a cobalt–carbide analog, but no peaks related to the bulk cobalt carbide were observed (Figure 2). A similar phenomenon was reported in a previous study, which showed that the Co XPS of the graphene-supported single Co atoms have two main Co 2p peaks at 780.9 and 796.2 eV with the peak spacing of 15.4 eV and shake-up satellite peaks, indicating that the single Co atoms coordinate with oxidation states [45]. The isolated Co atoms doped in the graphene matrix mainly form multifarious bonding configurations with the surrounding C, and the N and O heteroatoms mediate the Co atoms in oxidation states. Thus, the binding energy of the single Co atoms is larger than that of bulk cobalt carbide. Therefore, the Co^{2+} and Co^{3+} peaks of $Co_{2.5}$/rGO in Figure 2a correspond to isolated Co atoms (CoC_x) and CoO_x nanoparticles.

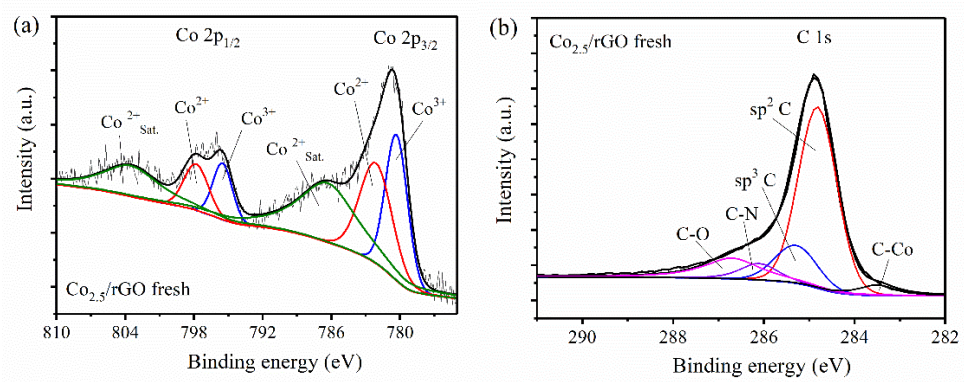

Figure 2. XPS characterization of $Co_{2.5}$/rGO catalyst: (**a**) energy spectrum of Co 2p; (**b**) energy spectrum of C1s.

The C 1s spectrum of the $Co_{2.5}$/rGO catalyst (Figure 2b) splits into several components. The main peak at 284.5 eV corresponds to the sp^2 C in graphene [46], indicating that most of the C atoms form conjugated honeycomb lattices of graphene. The peak at approximately 285.3 eV is assigned to sp^3 C, which originates from the lattice defects and edges of the graphene sheets [46]. The peaks from 286 eV to 288 eV correspond to the C−N and C−O bonds [41,46]. The small peak approximately around 283.3 eV is attributed to the carbidic C 1s signal [44], which in turn is attributed to the C atoms bonded with isolated Co atoms of the $Co_{2.5}$/rGO catalyst.

3.1.3. Raman

Figure 3 compares the Raman spectra of graphite, rGO, and $Co_{2.5}$/rGO. Highly ordered graphite has a G-band peak at approximately 1580 cm^{-1}, corresponding to the in-phase vibration of the sp^2 carbon lattice, and a weak D-band peak at approximately 1350 cm^{-1}, corresponding to the sp^3 carbons caused by the defects on the graphite edges [47]. The rGO material contains a significant fraction of the sp^3 amorphous carbons mainly generated by edges and lattice defects, and thus the rGO sample shows a noticeable D band. The ratio of the peak intensity of the D band to that of the G band (I_D/I_G) is inversely proportional to the perfection of the graphene's honeycomb lattice [47,48]. As shown in Figure 3, the I_D/I_G value of the $Co_{2.5}$/rGO catalyst is close to that of the rGO support, confirming that

the isolated Co atoms do not attack the pristine sp^2 carbon lattice of graphene but are embedded in the defective positions as substitutional or interstitial dopants through the construction of "metal vacancy" heterostructures. Hence, rGO with appropriate lattice defects is an ideal substrate for anchoring isolated Co atoms.

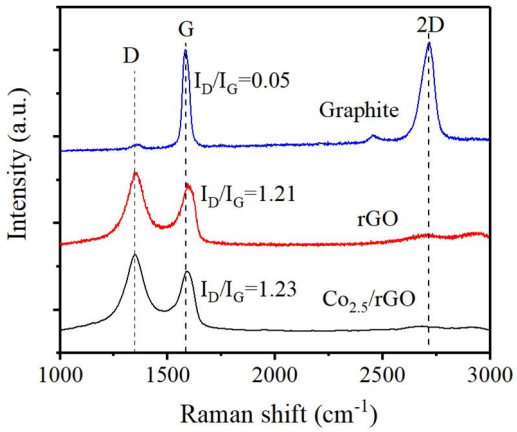

Figure 3. Raman diagrams of graphite, rGO, and $Co_{2.5}$/rGO catalyst.

3.1.4. XRD

The crystal structures of graphite, rGO, and $Co_{2.5}$/rGO were investigated through XRD analysis (Figure 4). Graphite has a sharp peak at a 2 theta of 26.4°, corresponding to the (002) plane of graphite (JCPDS PDF card: 41-1487). The XRD pattern of rGO shows trace amounts of graphite (002) diffraction signals with a widened peak and a low-degree-shift 2 theta, showing that rGO has a multilayer structure with increased lattice dimensions. The XRD peaks of the $Co_{2.5}$/rGO sample show a slightly enhanced and high-degree-shift 2 theta of the (002) plane compared with that of rGO, which is caused by the stacking thickness of the graphene layers during the preparation of the catalyst. In addition to the graphitic diffraction, the XRD pattern of the $Co_{2.5}$/rGO catalyst shows no diffraction signals corresponding to Co-related diffraction, indicating the small crystalline sizes and weak crystallinity of the Co species. This finding is in accordance with the TEM images (Figure 1a).

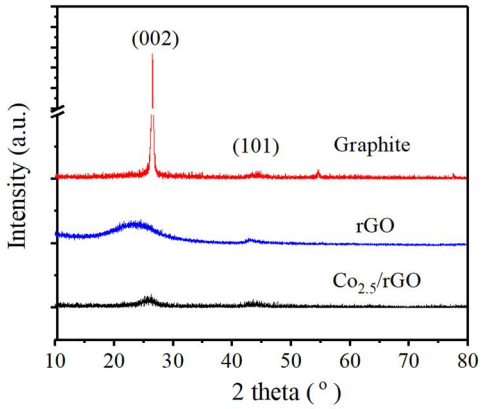

Figure 4. XRD patterns of graphite, rGO, and $Co_{2.5}$/rGO.

3.1.5. H_2-TPR

The TPR patterns of the $Co_{2.5}$/rGO catalyst are shown in Figure 5. rGO has certain oxygenic groups on its surface and periphery [49]. The hydrogenolysis of the –OH, –O–, and –COOH groups involves H_2 consumption starting at 400 °C. In the $Co_{2.5}$/rGO catalyst, rGO and Co oxides consume H_2. Moreover, according to the GC analysis, CH_4 exists in

the TPR exhaust gas (Figure 5b). Thus, the H_2 consumption of the $Co_{2.5}$/rGO sample includes the decomposition of oxygenic groups from rGO, reduction of Co oxides, and formation of CH_4. The multipeak reduction of Co oxides corresponds to the step–step reduction of Co_2O_3/Co_3O_4 to CoO and CoO to metallic Co [50]. A mixture of metallic Co powder (pre-reduced from CoO_x powder) and rGO cannot generate CH_4 at a temperature of approximately 530 °C; therefore, the formation of CH_4 is a representative feature of the $Co_{2.5}$/rGO sample during the H_2-TPR test. We speculate that the single Co atoms embedded in the graphene plane catalyze the bonded C atoms of rGO to form CH_4.

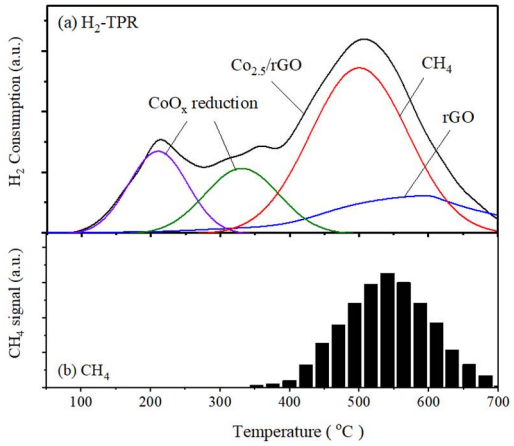

Figure 5. H_2-TPR patterns of $Co_{2.5}$/rGO (**a**) and CH_4 in the TPR exhaust gas (**b**).

3.1.6. Elemental Analyses

The three graphene materials, rGO, rGO*, and Gr, have similar specific surface areas but different elemental compositions (Table 1). The O atoms mainly come from the oxygenic groups, such as –OH and –COOH. The H atoms originate from the dangling H atoms for the termination of the dangling bonds of the graphene sheet edges, defects, and some groups. The rGO and rGO* materials have similar C, H, and O contents, but rGO contains 3.7 mol% N atoms. N was incorporated into the rGO network through the hydrothermal reduction of GO using hydrazine hydrate and ammonia as reducing reagents [51]. The comparison of rGO with Gr shows that rGO contains more H than Gr dose. More H indicates more lattice defects because the C dangling bonds are terminated by the H atoms.

Table 1. Property of graphene materials.

Entry	Support	S_{BET} ($m^2 \cdot g^{-1}$)	Element Composition (mol%)				Molar Ratio
			C	H	O	N	C:H:O:N
1	rGO	506	70.3	16.0	10.0	3.7	100:23:14:5
2	rGO*	516	70.1	17.6	12.2	0	100:25:17:0
3	Gr	583	84.7	7.2	7.1	1.0	100:9:8:1

3.2. Catalyst Investigation

3.2.1. Possible Reaction Pathway

GUA contains C_{aryl}–OH, C_{aryl}–OCH_3, and C_{aryl} O–CH_3 bonds and an aromatic ring in its structure. The catalytic conversion of GUA may generate a wide range of products over metal catalysts, including those formed without oxygen removal, partial oxygen removal, and complete oxygen removal. These products are generated by different reaction pathways, such as hydrogenation (HYD), demethoxylation (DMO), and dehydration (DHY). The possible reaction pathways for the HDO of GUA were explored based on the product distributions. As shown in Scheme 1, the main pathway involves the cleavage of C_{aryl}–

OCH_3 bond to phenol (Ph) through HYD and DMO followed by the saturation of the aromatic ring to CYHAOL through HYD; the other involves the saturation of the aromatic ring to 2-methoxycyclohexanol (MOCYHOL) through HYD and then the cleavage of C_{alkyl}–OCH_3 bond to CYHAOL. The DHY of CYHAOL generates a CYHA by-product.

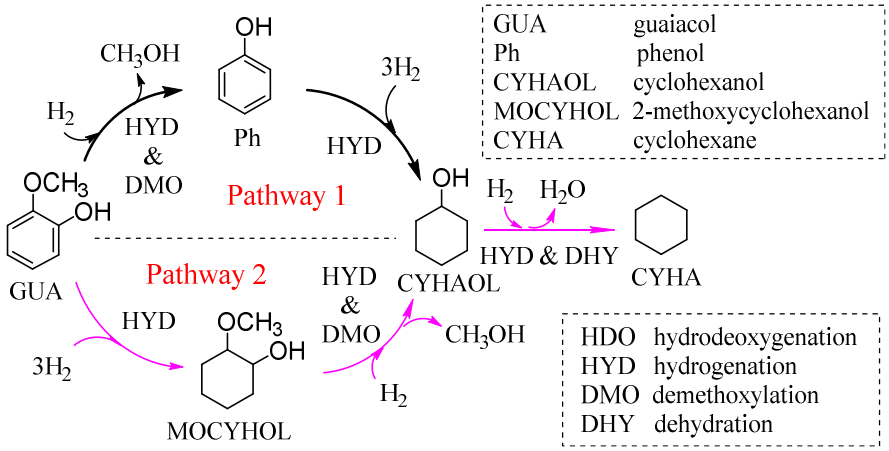

Scheme 1. Possible reaction pathways in the HDO of GUA over the Co/rGO catalyst.

3.2.2. Catalyst Screening Study

The catalysts' performance for HDO of GUA depends on two types of active sites: one is the metal-like site that readily activates hydrogen, while the other type of site nearby, such as an acid site, is responsible for the C-O bond activation [6,52]. For screening the functional catalyst, Fe, Co and Ni supported on rGO, and Co supported on different supports were tested in HDO of GUA. The catalytic performance of the prepared catalysts is presented in Table 2. Fe, Co, and Ni are eight-group elements with outer electronic structures of $3d^64s^2$, $3d^74s^2$, and $3d^84s^2$, respectively, and the three corresponding catalysts have similar specific surface areas but different catalytic activities (Table 1, entries 1–3). When the reaction occurs over the $Co_{2.5}$/rGO catalyst at 200 °C and 1.0 MPa H_2 pressure for 2 h, GUA is completely converted, and the yield of CYHAOL reaches 93.2 mol%. The $Ni_{2.5}$/rGO catalyst achieves 90.1 mol% conversion with 62.4 mol% and 35.1 mol% selectivity to CYHAOL and MOCYHOL, respectively. Ni catalysts usually catalyze total HYD to MOCYHOL as a major side reaction, especially at lower reaction temperatures [26]. The $Fe_{2.5}$/GO catalyst only converts 1.8 mol% of GUA. CYHA as a by-product is rarely detected in the reaction catalyzed by $Co_{2.5}$/rGO; therefore, Co is the most suitable transition metal to be supported on rGO for HDO reaction.

Table 2. HDO of GUA over the prepared catalysts [a].

Entry	Catalyst	S_{BET} ($m^2 \cdot g^{-1}$)	Conversion (mol%) GUA	Yield (mol%) CYHAOL	Selectivity (mol%)				
					Ph	CYHAOL	MOCYHOL	CYHA	Others [b]
1	$Co_{2.5}$/rGO	337	100	93.2	-	93.2	4.0	-	2.8
2	$Ni_{2.5}$/rGO	338	90.1	56.7	-	62.4	35.1	0.6	1.9
3	$Fe_{2.5}$/rGO	328	1.8	0.6	38.8	51.5	-	-	9.7
4	$Co_{2.5}/Al_2O_3$	413	-	-	-	-	-	-	-
5	$Co_{2.5}$/HY	572	2.2	1.4	32.2	63.2	-	-	4.6
6	CoO_x+rGO [c]		2.7	-	-	-	-	-	-
7	$Co_{2.5}$/rGO*	349	85.0	59.5	15.4	70.0	4.2	-	10.4
8	$Co_{2.5}$/Gr	341	20.5	7.8	46.7	38.0	7.7	-	7.6

[a] Reaction conditions: 300 mg of GUA in 10 mL of n-dodecane; catalyst loading = 30 mg (10 wt.% with respect to GUA); 200 °C; 1 MPa H_2; 2 h; GUA–guaiacol, CYHAOL–cyclohexanol, Ph–phenol, MOCYHOL–2-methoxycyclohexanol, CYHA–cyclohexane; [b] unidentified and unlisted product mixtures were labeled as "Others"; [c] 30 mg of CoO_x and 30 mg of rGO.

The support material is another decisive factor for determining catalyst activity. Compared with the $Co_{2.5}$/rGO catalyst, the $Co_{2.5}/Al_2O_3$ and $Co_{2.5}$/HY samples (Table 2, entries 4 and 5) show much lower activities. In general, a pristine metal species is an active component in the hydrogenation reaction; thus, the catalysts are prereduced or originally contain metals before they are used in GUA hydrogenation [13–26]. In this study, all the catalysts were used without prereduction treatments. Co in the $Co_{2.5}/Al_2O_3$ and $Co_{2.5}$/HY catalysts is in an oxide state, and thus, the catalysts exhibit extremely low activities because of insufficient metallic Co. However, the Co species in $Co_{2.5}$/rGO contains no metallic Co according to the HRTEM, XPS, and XRD characterization results, and the catalyst was used without prereduction treatment. $Co_{2.5}$/rGO was directly exposed to air during collection and weighing. Therefore, the active sites of $Co_{2.5}$/rGO are different from the frequently used type of catalysts requiring reduction treatment. Transition metal carbides, which are prepared by incorporating carbon atoms into the lattices of transition metals, have been demonstrated as promising catalysts for biomass conversions, especially in the C-C, C-O-C, and C-O-H bonds cleavage reactions [53]. We speculate that the catalytic component of $Co_{2.5}$/rGO for hydrogenation originates from a Co–carbide analog (CoC_x) formed by embedding Co single atoms in the graphene matrix. The poor reaction result over the physical CoO_x + rGO mixture (Table 2, entry 6) confirms the critical role of the CoC_x sites in hydrogenation catalysis. Thus, rGO as a support is involved in the construction of the CoC_x sites, whereas Al_2O_3 and HY support lack such functions.

The above results indicate that using rGO as a support is one of the decisive factors in determining the performance of the $Co_{2.5}$/rGO catalyst. According to the elemental analysis results (Table 1), rGO* is an N-free material, and rGO contains 3.7 mol% N. $Co_{2.5}$/rGO* (Table 2, entry 7) achieves 85.0 mol% conversion and 59.5 mol% CYHAOL yield, manifesting that the doped N atoms are not an indispensable factor in catalytic function. However, the improved activity of the $Co_{2.5}$/rGO catalyst as compared with that of $Co_{2.5}$/rGO* confirms a positive role of N doping in graphene. Transition metal nitrides have been explored in HDO conversions [28]. Moreover, the N atoms merged within the graphene matrix disrupt the electronic neutrality of adjacent carbon atoms [54,55], which manipulate the electronic status of CoC_x and CoO_x in higher electronic density. This effect improves the activity of the $Co_{2.5}$/rGO catalyst. The O functional groups of rGO may improve the dispersion and stability of the supported CoO_x nanoparticles through an anchoring effect during impregnation and calcination. In brief, rGO with appropriate amounts of N and O heteroatoms is a suitable graphene material as a support.

In order to confirm the hypothesis that the hydrogenation function of $Co_{2.5}$/rGO is provided by CoC_x, the $Co_{2.5}$/Gr catalyst prepared with a commercial graphene (Gr) was investigated for clarity. The conversion and CYHAOL yield over $Co_{2.5}$/Gr (Table 1, entry 8) is much less than that over $Co_{2.5}$/rGO. The catalyst-specific surface area of $Co_{2.5}$/Gr is 341 $m^2 \cdot g^{-1}$, and the average particle size of CoO_x nanoparticles on Gr surface (Figure S2a) is 6.5 nm, which indicates that the low activity of $Co_{2.5}$/Gr is not caused by the small specific surface area and the low dispersion of CoO_x components. Supposing the hydrogenation function of $Co_{2.5}$/rGO derives from the in situ reduction of CoO_x nanoparticles to metallic Co during reaction, then $Co_{2.5}$/Gr should be as good—or as bad—as $Co_{2.5}$/rGO; therefore, some critical factors determine the catalysts' performance. The biggest difference between rGO and Gr is that rGO can anchor more single-metal atoms than Gr does. The evidence is shown in the HAADF-STEM image of $Co_{2.5}$/rGO. (Figure 1e) shows the high-density distribution of the isolated Co atoms in the graphene matrix, while the number of the isolated Co atoms decreases considerably in the image of $Co_{2.5}$/Gr (Figure S2b). The more Co single atoms in the graphene matrix, the more Co–carbide analog (CoC_x) the catalyst contains. Transition metal carbides have been compared to platinum group metals, showing similar catalytic properties, which means that they could be promising catalysts for HDO reactions [52]; therefore, $Co_{2.5}$/Gr exhibits weak catalytic activity due to the low population of the CoC_x sites.

The data in entry 6 of Table 2 show that CoO_x fails to conduct the HDO of GUA without the participation of CoC_x; however, the CoO_x nanoparticles on rGO surface may improve the ability of the $Co_{2.5}$/rGO catalyst to break C_{aryal}–OCH_3 bond. HDO was proposed to need a bifunctional catalyst where acid sites are required for C–O bond activation, allowing easier C–O scission [6]. CoO_x contains acidity according to the NH_3-TPD result (Figure S3a) and can adsorb the oxygenic groups in a GUA molecule through acid–base-pairing interactions, facilitating the cleavage of the C–O bond. Therefore, CoO_x, in combination with CoC_x, plays a role in establishing the metal−acid bifunction of the catalyst. A similar bifunctional catalyst was established for HDO reaction based on molybdenum carbide and oxide [56]. When Ph and CYHAOL are used as feedstock and the reaction is run at 200 °C and 1 MPa H_2 for 2 h, Ph is completely converted to CYHAOL over the $Co_{2.5}$/rGO catalyst, whereas CYHAOL is almost not converted. Cleavage of the C_{aryl}–OH bond needs strong acidic components such as HZSM-5 zeolite [2,28], while the mild acid of CoO_x appropriately avoids cleaving the C_{aryl}–OH bond. In this reaction, especially carried out in milder conditions, the basicity of support can affect the selectivity of bond breaking [6,57,58]. The presence of base promotes the demethoxylation step and suppresses the unselective C-O dissociation [57]. The basicity of CoO_x is not obvious according to the CO_2-TPD result (Figure S3b), but N doping incorporates basic sites in the graphene texture [26], which potentially favors the C_{aryl}–OCH_3 bond cleavage, making the $Co_{2.5}$/rGO catalyst has good selectivity to CYHAOL. Scheme 2 shows the main catalysis in the selective HDO of GUA to CYHAOL over the $Co_{2.5}$/rGO catalyst, in which Ph is used as the intermediate. H_2 dissociates to active H species on the CoC_x sites; the C_{aryl}–OCH_3 bond of GUA is activated by the oxophilic acid sites of CoO_x and dissociated by active H. The metal–acid bifunction of the $Co_{2.5}$/rGO catalyst in the HDO of GUA to CYHAOL is attributed to the unique synergy between the CoC_x sites and the acid sites of the CoO_x nanoparticles. The $Co_{2.5}$/rGO catalyst selectively saturates the aromatic ring and dominantly cleaves C_{aryl}–OCH_3 bond in the GUA. These processes result in a good performance in CYHAOL production.

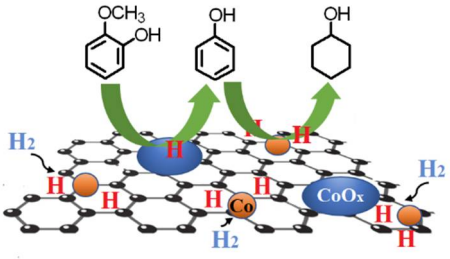

Scheme 2. Possible reaction mechanism of HDO of GUA over the $Co_{2.5}$/rGO catalyst with Ph as the intermediate.

3.2.3. Optimization of Catalyst Preparation Conditions

The effects of the Co loading and calcination temperature on the Co/rGO catalysts were studied. The results are shown in Figure 6. Co/rGO catalysts with different Co loadings were prepared for the HDO of GUA (Figure 6a). When the Co loading increases from 1.0 mmol/g to 2.5 mmol/g, the yield of CYHAOL constantly increases and reaches 93.2 mol% at 2.5 mmol/g; further increase in Co loading has little contribution to the CYHAOL yield. Figure 6b shows the results obtained for the $Co_{2.5}$/rGO catalysts at different calcination temperatures in N_2. The conversion of GUA and the yield of CYHAOL shows volcano-like shapes when the calcination temperature is increased from 400 °C to 700 °C, achieving maximum values at 500 °C. The $Co_{2.5}$/rGO catalyst calcinated at 400 °C in N_2 only leads to 4.6 mol% conversion of GUA. When the calcination temperature is above 500 °C, the aggregation of nanoparticles becomes obvious, as evidenced by the low specific surface areas of the samples calcined at 600 °C and 700 °C. The highest efficiency for the HDO of GUA was obtained using a catalyst with a loading of 2.5 mmol Co per gram of rGO at a calcination temperature of 500 °C.

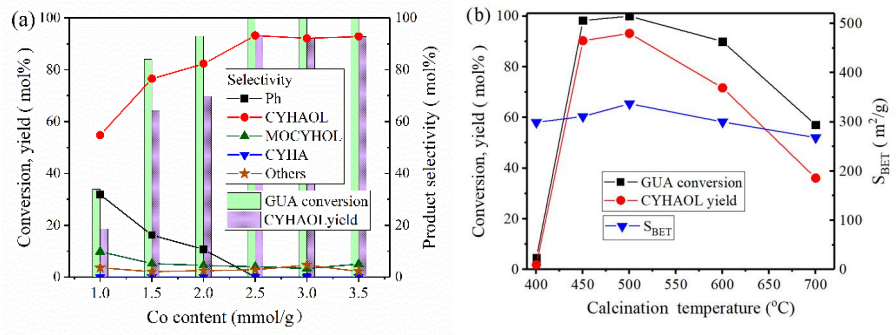

Figure 6. Influence of catalyst preparation conditions on HDO of GUA reactions: (**a**) Co loading amounts; (**b**) catalyst calcination temperature (reaction conditions: 300 mg of GUA in 10 mL of n-dodecane; catalyst loading = 30 mg; 200 °C; 1 MPa H_2; 2 h).

Blanco et al. [26] prepared the Co/GOr and Co/GOr-N catalysts by wet impregnation of Co over reduced graphene oxide undoped and doped with N, calcination in N_2 at 350 °C and reduction under H_2 at 300 °C. As evidenced by the XRD pattern and CO chemisorption of the catalysts, the hydrogenation sites of Co/rGOr and Co/rGOr-N are metallic Co (Co^0) components. In our study, the $Co_{2.5}$/rGO catalyst calcinated at 500 °C in N_2 and used without H_2-reduction pretreatment exhibits good activity. Metallic oxides or nitrates on carbonaceous supports may form metals by carbothermal reduction during calcination in inert gases. For example, NiFe alloy nanoparticles were prepared by calcination of a cellulose filter paper impregnated with Fe and Ni nitrates at 800 °C for 2 h under N_2 [59]. The $Co_{2.5}$/rGO catalyst calcinated at 500 °C in N_2 does not contain metallic Co according to the XRD pattern and the lattice fringes in the HRTEM image of the catalyst. Therefore, the CoC_x sites of $Co_{2.5}$/rGO serve as the activity sites. The low activity of the $Co_{2.5}$/rGO catalyst calcined at 400 °C in N_2 manifests that the calcination temperature at 400 °C or below cannot provide sufficient energy for the formation of the CoC_x sites, so the Co/GOr and Co/GOr-N catalysts calcinated at only 350 °C [26] can hardly contain the CoC_x sites.

3.2.4. Effects of Reaction Conditions

Figure 7 shows the variations in GUA conversion and product distribution among different reaction conditions. As reaction time proceeds, GUA conversion rate increases rapidly and reaches 100 mol% at 2 h. Selectivity to the Ph intermediate product gradually decreases over time after the initial accumulation, accompanied by an increase in selectivity to CYHAOL. This result shows that Ph is an intermediate progressing toward CYHAOL. An increase in reaction temperature from 160 °C to 200 °C increases the conversion rate of GUA and yield of CYHAOL. When the reaction approaches the 100 mol% conversion, the improved reaction temperature slightly decreases the CYHAOL yield, indicating that CYHAOL is relatively stable over the temperature range from 200 °C to 240 °C. With increasing H_2 pressure from 0.25 MPa to 4.0 MPa, the CYHAOL yield reaches 93.2 mol% at 1.0 MPa and then decreases gradually with pressure, and selectivity to MOCYHOL increases. These effects indicate that high H_2 pressure intensifies the HYD saturation of the aromatic ring to form MOCYHOL. Theoretically, MOCYHOL should proceed toward CYHAOL through the cleavage of C_{alkyl}-OCH_3 bond. However, the fully hydrogenated MOCYHOL is more stable than Ph, and the higher steric hindrance of MOCYHOL restrains the cleavage of C_{alkyl}-OCH_3 bond. Therefore, the GUA–Ph–CYHAOL pathway is much more conducive to producing MOCYHOL than the GUA–MOCYHOL–CYHAOL pathway, and a lower H_2 pressure facilitates CYHAOL formation.

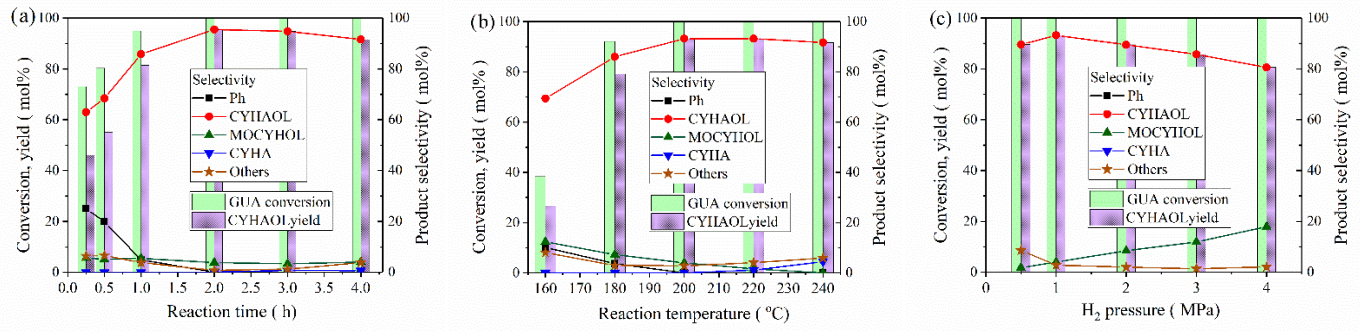

Figure 7. Influence of (**a**) reaction time, (**b**) reaction temperature, and (**c**) H_2 pressure on the HDO of GUA (Reaction conditions: 300 mg of GUA in 10 mL of n-dodecane, catalyst loading = 30 mg. Other conditions: (**a**) 200 °C, 1 MPa H_2; (**b**) 1 MPa H_2, 2 h; (**c**) 200 °C, 2 h).

3.2.5. Catalyst Recycle Study

Catalyst stability is a critical factor in developing conversion processes industrially. Sintering and leaching of metal components are major problems for liquid-phase HDO reactions [60]. Further, coking on the catalyst and structural degradation leads to the deactivation of the catalysts [60]. Figure 8 summarizes the characterization results of the spent $Co_{2.5}$/rGO catalyst. The TEM image of the spent $Co_{2.5}$/rGO catalyst shows the homogenous dispersion of nanoparticles (Figure 8a) with a slightly larger average size of 7.6 nm (Figure 8b) as compared to that of a fresh one (6.7 nm). Fresh $Co_{2.5}$/rGO catalyst contains no metallic Co (Figure 2a) and is used without prereduction treatment. A hypothesis states that $Co_{2.5}$/rGO catalysts undergo in situ reduction to form metallic Co. However, the XPS spectra of the spent catalyst (Figure 8c) show no metallic Co, thereby confirming that the active sites for activating H_2 is CoC_x rather than metallic Co. Figure 8d shows the TG curves of the fresh and spent $Co_{2.5}$/rGO catalysts. The weight loss rates mainly relate to the burning of rGO at approximately 310 °C, and the coke, if present, cannot be identified because it burnt with rGO together. However, a careful comparison of the two curves found that the weight loss of the spent catalyst is about 3% higher than that of the fresh one, which is caused by coke deposition on the spent catalyst. Figure 8e,f show the high density of isolated Co atoms in the graphene nanosheet of the spent catalyst.

The reusability of the $Co_{2.5}$/rGO catalyst was investigated during the HDO of the GUA (Figure 9). The catalyst recycling experiment was performed without regeneration. The conversion rate of GUA drops to 70.4 mol% in the repeated test (cycle 2), indicating the deactivation of the $Co_{2.5}$/rGO catalyst. One concern regarding the causes of deactivation is that single Co atoms in the graphene matrix may move and aggregate during the thermodynamic process of a reaction, which leads to the loss of CoC_x sites. A model reaction was performed to exclude this possibility. The fresh $Co_{2.5}$/rGO catalyst was first processed under the following conditions: 10 mL of n-dodecane, 30 mg of the catalyst, 200 °C, and 1 MPa H_2 for 2 h. Then, 300 mg of GUA was added to the reactor, and the reaction proceeded under the same conditions. The result of "Pretreated" in Figure 9 shows that the catalyst maintains its activity, indicating that the single Co atoms embedded in the rGO lattice are stable under the reaction conditions, in accordance with the image of HAADF-STEM (Figure 8f). Thereby, coking is the main reason for the deactivation of the catalyst. Coking was also presented in previous studies on the catalytic HDO of GUA [21,60–63].

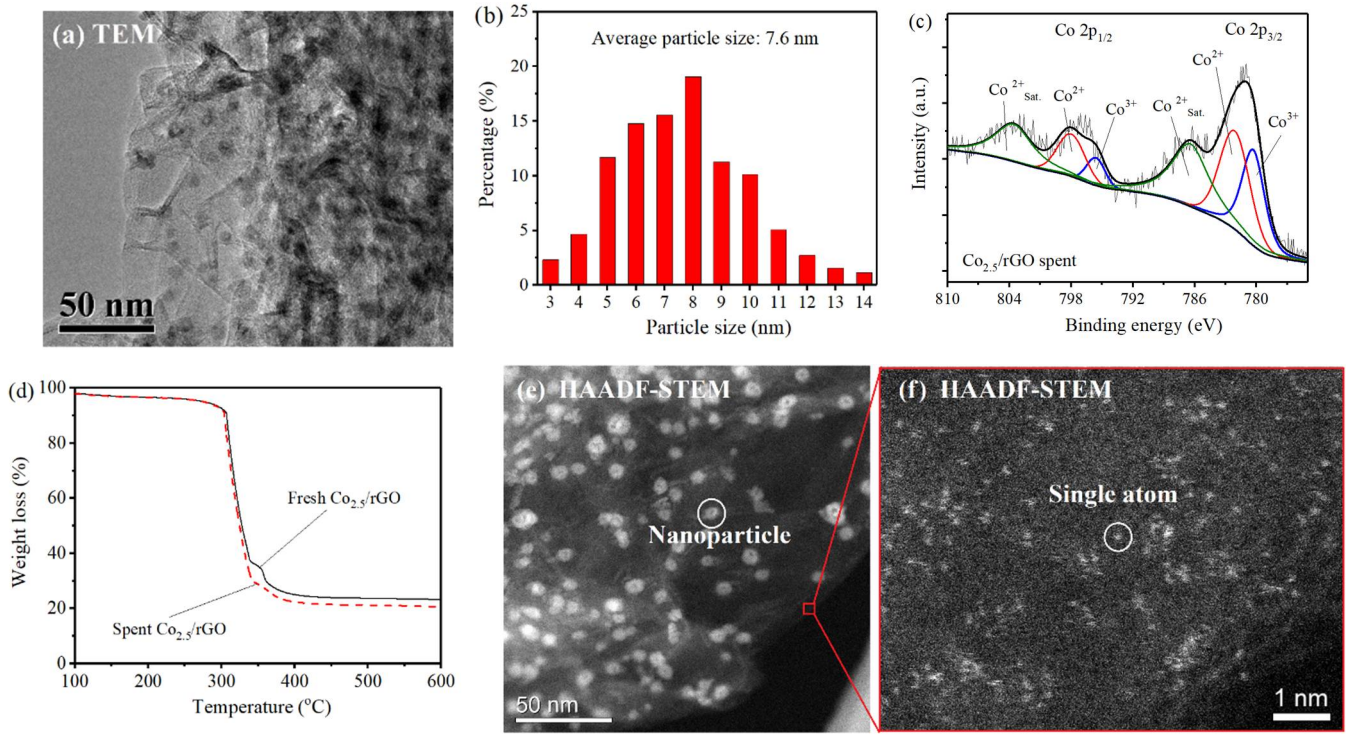

Figure 8. Characterization results of the spent $Co_{2.5}$/rGO catalyst: (**a**) TEM image; (**b**) particle size distribution; (**c**) energy spectrum of Co 2p in XPS result; (**d**) TG/DTA image; (**e**,**f**) HAADF-STEM images.

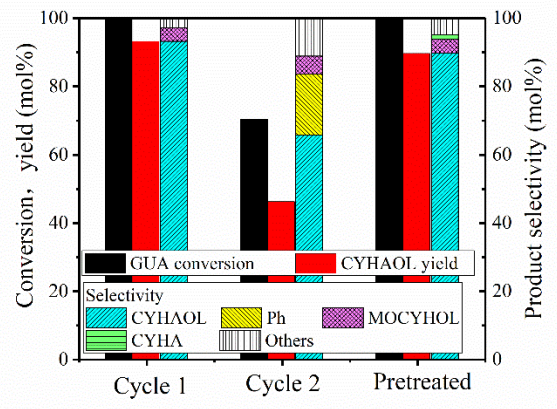

Figure 9. Reuse of $Co_{2.5}$/rGO in HDO of GUA to CYHAOL (reaction conditions: 300 mg of GUA in 10 mL of n-dodecane; catalyst loading = 30 mg; 200 °C; 1 MPa H_2; 2 h).

4. Conclusions

The catalytic HDO of GUA, a phenolic model compound of biomass lignin pyrolysis products, was investigated over Co/rGO catalysts synthesized through a practical impregnation–calcination approach. A series of characterization results revealed that the prepared Co/rGO catalyst contains single Co atoms embedded in the graphene matrix and CoO_x nanoparticles on the graphene surface. The isolated Co atoms formed stable metal carbide analogs (CoC_x) with rGO when the catalyst was calcined at 500 °C in N_2. The graphene texture is a decisive factor in determining the catalyst performance. rGO with proper N heteroatoms and lattice defects is a suitable material for catalyst fabrication. The optimized Co/rGO catalyst without prereduction treatment led to the complete conversion of GUA with 93.2% yield to CYHAOL under mild reaction conditions (200 °C and 1.0 MPa H_2 pressure for 2 h). The catalytic HDO of GUA to GYHAOL mainly occurred through

the pathway using phenol as the intermediate. The Co/rGO catalyst possesses metal–acid bifunctional characteristics, by which the CoC_x sites readily activate H_2 and provide active H, and the CoO_x nanoparticles provide acid sites that are required to activate the C–O bond, allowing easier C–O scission by active H. The isolated Co atoms of the Co/rGO catalyst were stable under the reaction conditions of 200 °C and 1.0 MPa H_2, which emphasized the feasibility of constructing the highly dispersed metal–carbide species through embedding single metal atoms in the graphene matrix.

Supplementary Materials: The following supporting information can be downloaded at: https://www.mdpi.com/article/10.3390/nano12193388/s1, including the characterization description; Figure S1: The full-scan XPS survey spectrum of the $Co_{2.5}$/rGO catalyst; Figure S2: Characterization results of the $Co_{2.5}$/Gr catalyst: (a) TEM image and particle size distribution, (b) HAADF-STEM image; Figure S3: The NH_3-TPD result of the CoO_x powder; Table S1: Catalysts for hydrodeoxygenation of guaiacol to cyclohexanol; Table S2: Co-based catalysts used in hydrodeoxygenation of guaiacol. References [8,9,13–32] are cited in the Supplementary Materials.

Author Contributions: Conceptualization: Q.G. and J.Z.; writing—original draft preparation: Q.G.; Investigation: Q.G. and J.M.; validation: J.M. (TEM, HAADF-STEM, and Raman data) and Y.L. (H_2-TPR and XRD data); writing—review and editing: S.L., J.Y. and J.Z.; supervision: J.Z. All authors have read and agreed to the published version of the manuscript.

Funding: This work was supported by the National Natural Science Foundation of China (Grant No. 21975035) and the Support Program for Excellent Talents in colleges and universities in Liaoning province (Grant No. LR2020079).

Institutional Review Board Statement: Not applicable.

Informed Consent Statement: Not applicable.

Data Availability Statement: Not applicable.

Conflicts of Interest: The authors declare no conflict of interest.

References

1. Li, C.Z.; Zhao, X.C.; Wang, A.; Huber, G.W.; Zhang, T. Catalytic transformation of lignin for the production of chemicals and fuels. *Chem. Rev.* **2015**, *115*, 11559–11624. [CrossRef]
2. Duan, H.N.; Tian, Y.J.; Gong, S.Y.; Zhang, B.F.; Lu, Z.J.; Xia, Y.Q.; Shi, Y.W.; Qiao, C.Z. Effects of Crystallite Sizes of Pt/HZSM-5 Zeolite Catalysts on the Hydrodeoxygenation of Guaiacol. *Nanomaterials* **2020**, *10*, 2246. [CrossRef]
3. Saidi, M.; Samimi, F.; Karimipourfard, D.; Nimmanwudipong, T.; Gates, B.C.; Rahimpour, M.R. Upgrading of lignin-derived bio-oils by catalytic hydrodeoxygenation. *Energy Environ. Sci.* **2014**, *7*, 103–129. [CrossRef]
4. Chen, Z.Y.; Kukushkin, R.G.; Yeletsky, P.M.; Saraev, A.A.; Bulavchenko, O.A.; Millan, M. Coupling Hydrogenation of Guaiacol with In Situ Hydrogen Production by Glycerol Aqueous Reforming over Ni/ Al_2O_3 and Ni-X/Al_2O_3 (X = Cu, Mo, P) Catalysts. *Nanomaterials* **2020**, *10*, 1420. [CrossRef] [PubMed]
5. Zhang, P.; Sun, Y.; Lu, M.H.; Zhu, J.; Li, M.S.; Shan, Y.H.; Shen, J.Y.; Song, C.S. High-loading nickel phosphide catalysts supported on SiO_2–TiO_2 for hydrodeoxygenation of guaiacol. *Energy Fuels* **2019**, *33*, 7696–7704. [CrossRef]
6. Kim, S.; Kwon, E.E.; Kim, Y.T.; Jung, S.; Kim, H.J.; Huber, G.W.; Lee, J. Recent advances in hydrodeoxygenation of biomass-derived oxygenates over heterogeneous catalysts. *Green Chem.* **2019**, *21*, 3715–3743. [CrossRef]
7. Nakagawa, Y.; Ishikawa, M.; Tamura, M.; Tomishige, K. Selective production of cyclohexanol and methanol from guaiacol over Ru catalyst combined with MgO. *Green Chem.* **2014**, *16*, 2197–2203. [CrossRef]
8. Han, G.H.; Lee, M.W.; Park, S.; Kim, H.J.; Ahn, J.P.; Seo, M.; Lee, K.Y. Revealing the factors determining the selectivity of guaiacol HDO reaction pathways using ZrP-supported Co and Ni catalysts. *J. Catal.* **2019**, *377*, 343–357. [CrossRef]
9. Mei, X.; Wu, D.F. Highly selective catalytic conversion of lignin-derived phenolic compounds to cycloalkanes over a hierarchically structured zeolite catalyst. *J. Mater. Sci.* **2019**, *54*, 2940–2959.
10. Lu, M.H.; Sun, Y.; Zhang, P.; Zhu, J.; Li, M.S.; Shan, Y.H.; Shen, J.Y.; Song, C.S. Hydrodeoxygenation of guaiacol catalyzed by high-loading Ni catalysts supported on SiO_2–TiO_2 binary oxides. *Ind. Eng. Chem. Res.* **2019**, *58*, 1513–1524. [CrossRef]
11. Niu, X.P.; Feng, F.X.; Yuan, G.; Zhang, X.W.; Wang, Q.F. Hollow MFI zeolite supported Pt catalysts for highly selective and stable hydrodeoxygenation of guaiacol to cycloalkanes. *Nanomaterials* **2019**, *9*, 362. [CrossRef] [PubMed]
12. Zhao, Y.P.; Wu, F.P.; Song, Q.L.; Fan, X.; Jin, L.J.; Wang, R.Y.; Cao, J.P.; Wei, X.Y. Hydrodeoxygenation of lignin model compounds to alkanes over Pd–Ni/HZSM-5 catalysts. *J. Energy Inst.* **2020**, *93*, 899–910. [CrossRef]
13. Wang, X.C.; Wu, P.X.; Wang, Z.Q.; Zhou, L.L.; Liu, Y.C.; Cheng, H.Y.; Arai, M.; Zhang, C.; Zhao, F.Y. Chlorine-modified Ru/TiO_2 catalyst for selective guaiacol hydrodeoxygenation. *ACS Sustain. Chem. Eng.* **2021**, *9*, 3083–3094. [CrossRef]

14. Kim, M.; Ha, J.M.; Lee, K.Y.; Jae, J. Catalytic transfer hydrogenation/hydrogenolysis of guaiacol to cyclohexane over bimetallic RuRe/C catalysts. *Catal. Commun.* **2016**, *86*, 113–118. [CrossRef]
15. Long, W.; Liu, P.L.; Xiong, W.; Hao, F.; Luo, H.A. Conversion of guaiacol as lignin model component using acid-treated, multi-walled carbon nanotubes supported Ru-MnO bimetallic catalysts. *Can. J. Chem.* **2020**, *98*, 57–65. [CrossRef]
16. Xu, Q.Q.; Shi, Y.S.; Yang, L.; Fan, G.L.; Li, F. The promotional effect of surface Ru decoration on the catalytic performance of Co-based nanocatalysts for guaiacol hydrodeoxygenation. *Mol. Catal.* **2020**, *497*, 111224–111233. [CrossRef]
17. Nguyen, T.S.; Laurenti, D.; Afanasiev, P.; Konuspayeva, Z.; Piccolo, L. Titania-supported gold-based nanoparticles efficiently catalyze the hydrodeoxygenation of guaiacol. *J. Catal.* **2016**, *344*, 136–140. [CrossRef]
18. Lu, M.H.; Jiang, Y.J.; Sun, Y.; Zhang, P.; Zhu, J.; Li, M.S.; Shan, Y.H.; Shen, J.Y.; Song, C.S. Hydrodeoxygenation of guaiacol catalyzed by ZrO_2-CeO_2 supported nickel catalysts with high-loading. *Energy Fuels* **2020**, *34*, 4685–4692. [CrossRef]
19. Lu, J.Q.; Liu, X.; Yu, G.Q.; Lv, J.K.; Rong, Z.M.; Wang, M.; Wang, Y. Selective hydrodeoxygenation of guaiacol to cyclohexanol catalyzed by nanoporous nickel. *Catal. Lett.* **2020**, *150*, 837–848. [CrossRef]
20. Liu, L.J.; Liu, Y.G.; Gao, X.; Zhang, R.Q.; Zhai, Y.P. Hydrodeoxygenation of bio-oil model compounds over amorphous NiB/SiO_2-Al_2O_3 catalyst in oil-water biphasic system. *J. Fuel Chem. Technol.* **2017**, *45*, 932–938. [CrossRef]
21. Dongil, A.B.; Pastor-Pérez, L.; Sepúlveda-Escribano, A.; García, R.; Escalona, N. Hydrodeoxygenation of guaiacol: Tuning the selectivity to cyclohexene by introducing Ni nanoparticles inside carbon nanotubes. *Fuel* **2016**, *172*, 65–69. [CrossRef]
22. López, M.; Palacio, R.; Royer, S.; Mamede, A.S.; Fernández, J.J. Mesostructured CMK-3 carbon supported Ni–ZrO_2 as catalysts for the hydrodeoxygenation of guaiacol. *Micropor. Mesopor. Mater.* **2020**, *292*, 09694–109694. [CrossRef]
23. Rong, Z.M.; Lu, J.Q.; Yu, G.Q.; Li, J.J.; Wang, M.; Zhang, S.F. Promoting selective hydrodeoxygenation of guaiacol over amorphous nanoporous $NiMnO_2$. *Catal. Commun.* **2020**, *140*, 105987–105991. [CrossRef]
24. Zhou, M.H.; Ye, J.; Liu, P.; Xu, J.M.; Jiang, J.C. Water-assisted selective hydrodeoxygenation of guaiacol to cyclohexanol over supported Ni and Co bimetallic catalysts. *ACS Sustain. Chem. Eng.* **2017**, *5*, 8824–8835. [CrossRef]
25. Chen, C.Z.; Zhou, M.H.; Liu, P.; Sharma, B.K.; Jiang, J.C. Flexible NiCo-based catalyst for direct hydrodeoxygenation of guaiacol to cyclohexanol. *New J. Chem.* **2020**, *44*, 18906–18916. [CrossRef]
26. Blanco, E.; Carrales-Alvarado, D.; Dongil, A.B.; Escalona, N. Effect of the Support Functionalization of Mono- and Bimetallic Ni/Co Supported on Graphene in Hydrodeoxygenation of Guaiacol. *Ind. Eng. Chem. Res.* **2021**, *60*, 18870–18879. [CrossRef]
27. Liu, X.; Jia, W.; Xu, G.; Zhang, Y.; Fu, Y. Selective Hydrodeoxygenation of Lignin-Derived Phenols to Cyclohexanols over Co-Based Catalysts. *ACS Sustain. Chem. Eng.* **2017**, *5*, 8594–8601. [CrossRef]
28. Liu, X.H.; Xu, L.J.; Xu, G.Y.; Jia, W.D.; Ma, Y.F.; Zhang, Y. Selective Hydrodeoxygenation of Lignin-Derived Phenols to Cyclohexanols or Cyclohexanes over Magnetic CoN_x@NC Catalysts under Mild Conditions. *ACS Catal.* **2016**, *6*, 7611–7620. [CrossRef]
29. Blanco, E.; Dongil, A.B.; Escalona, N. Synergy between Ni and Co nanoparticles supported on carbon in guaiacol conversion. *Nanomaterials* **2020**, *10*, 2199. [CrossRef]
30. Mora-Vergara, I.D.; Moscoso, L.H.; Gaigneaux, E.M.; Giraldo, S.A.; Baldovino-Medrano, V.G. Hydrodeoxygenation of guaiacol using NiMo and CoMo catalysts supported on alumina modified with potassium. *Catal. Today* **2018**, *302*, 125–135. [CrossRef]
31. Liu, G.H.; Zong, Z.M.; Liu, Z.Q.; Liu, F.J.; Zhang, Y.Y.; Wei, X.Y. Solvent-controlled selective hydrodeoxygenation of bio-derived guaiacol to arenes or phenols over a biochar supported Co-doped MoO_2 catalyst. *Fuel Process. Technol.* **2018**, *179*, 114–123. [CrossRef]
32. Gutierrez, A.; Turpeinen, E.M.; Viljava, T.R.; Krause, O. Hydrodeoxygenation of model compounds on sulfided CoMo/γ-Al_2O_3 and NiMo/γ-Al_2O_3 catalysts; Role of sulfur-containing groups in reaction networks. *Catal. Today* **2017**, *285*, 125–134. [CrossRef]
33. Alexander, A.M.; Hargreaves, J.S.J. Alternative Catalytic Materials: Carbides, Nitrides, Phosphides and Amorphous Boron Alloys. *Chem. Soc. Rev.* **2010**, *39*, 4388–4401. [CrossRef] [PubMed]
34. Zhong, L.; Yu, F.; An, Y.; Zhao, Y.; Sun, Y.; Li, Z.; Lin, T.; Lin, Y.; Qi, X.; Dai, Y.; et al. Cobalt Carbide Nanoprisms for Direct Production of Lower Olefins from Syngas. *Nature* **2016**, *538*, 84–87. [CrossRef]
35. Lv, Y.; Mao, J.B.; Wang, F.; Zhou, J.X. Review of application functions of graphene materials in catalysts. *Ind. Catal.* **2021**, *29*, 1–9.
36. Baby, A.; Trovato, L.; Valentin, C.D. Single atom catalysts (SAC) trapped in defective and nitrogen−doped graphene supported on metal substrates. *Carbon* **2021**, *174*, 772–788. [CrossRef]
37. Liu, J.G.; Sun, J.M.; Singhe, T.; Linc, S.; Ma, L. Facile synthesis of N-doped graphene encapsulated Ni@N/C catalyst and its catalysis for highly selective semi−hydrogenation of alkynes. *Green Chem. Eng.* 2022, *in press*. [CrossRef]
38. Zhou, J.X.; Wang, Y.; Guo, X.W.; Mao, J.B.; Zhang, S.G. Etherification of glycerol with isobutene on sulfonated graphene: Reaction and separation. *Green Chem.* **2014**, *16*, 4669–4679. [CrossRef]
39. Kovtyukhova, N.I.; Ollivier, P.J.; Martin, B.R.; Mallouk, T.E.; Chizhik, S.A.; Buzaneva, E.V.; Gorchinskiy, A.D. Layer-by-layer assembly of ultrathin composite films from micron-sized graphite oxide sheets and polycations. *Chem. Mater.* **1999**, *11*, 771–778. [CrossRef]
40. Guex, L.G.; Sacchi, B.; Peuvot, K.F.; Andersson, R.L.; Pourrahimi, A.M.; Ström, V.; Farris, S.; Olsson, R.T. Experimental review: Chemical reduction of graphene oxide (GO) to reduced graphene oxide (rGO) by aqueous chemistry. *Nanoscale* **2017**, *9*, 9562–9571. [CrossRef]
41. Zhang, Q.; Zhang, X.; Wang, J.; Wang, C. Topical Review: Graphene-supported Single-Atom Catalysts and Applications in Electrocatalysis. *Nanotechnology* **2021**, *32*, 032001–032024. [CrossRef] [PubMed]

42. Kim, G.; Jhi, S.H.; Lim, S.; Park, N. Effect of Vacancy Defects in Graphene on Metal Anchoring and Hydrogen Adsorption. *Appl. Phys. Lett.* **2009**, *94*, 173102. [CrossRef]
43. Fu, L.; Liu, Z.; Liu, Y.; Han, B.; Hu, P.; Cao, L.; Zhu, D. Beaded cobalt oxide nanoparticles along carbon nanotubes: Towards more highly integrated electronic devices. *Adv. Mater.* **2005**, *17*, 217–221. [CrossRef]
44. Zhang, T.F.; Wu, J.S.; Xu, Y.Q.; Wang, X.P.; Ni, J.; Li, Y.W.; Niemantsverdriet, J.W. Cobalt and cobalt carbide on alumina/NiAl(110) as a catalyst model. *Catal. Sci. Technol.* **2017**, *7*, 5893–5899. [CrossRef]
45. Li, M.; Wu, S.J.; Yang, X.Y.; Hu, J.; Peng, L.; Bai, L.; Huo, Q.S.; Guan, J.Q. Highly efficient single atom cobalt catalyst for selective oxidation of alcohols. *Appl. Catal. A–Gen.* **2017**, *543*, 61–66. [CrossRef]
46. Kovács, G.J.; Bertóti, I.; Radnóczi, G. X-ray photoelectron spectroscopic study of magnetron sputtered carbon–nickel composite films. *Thin Solid Films* **2008**, *516*, 7942–7946. [CrossRef]
47. Casiraghi, C.; Hartschuh, A.; Qian, H.; Piscanec, S.; Georgi, C.; Fasoli, A.; Novoselov, K.S.; Basko, D.M.; Ferrari, A.C. Raman spectroscopy of graphene edges. *Nano Lett.* **2009**, *9*, 1433–1441. [CrossRef]
48. Kudin, K.N.; Ozbas, B.; Schniepp, H.C.; Prud'homme, R.K.; Aksay, I.A.; Car, R. Raman spectra of graphite oxide and functionalized graphene sheets. *Nano Lett.* **2008**, *8*, 36–41. [CrossRef]
49. Rümmeli, M.H.; Rocha, C.G.; Ortmann, F.; Ibrahim, I.; Sevincli, H.; Börrnert, F.; Kunstmann, J.; Bachmatiuk, A.; Pötsche, M.; Shiraishi, M.; et al. Graphene: Piecing it together. *Adv. Mater.* **2011**, *23*, 4471–4490. [CrossRef]
50. Lin, H.Y.; Chen, Y.W. The mechanism of reduction of cobalt by hydrogen. *Mater. Chem. Phys.* **2004**, *85*, 171–175. [CrossRef]
51. Long, D.; Li, W.; Ling, L.; Miyawaki, J.; Mochida, I.; Yoon, S.H. Preparation of nitrogen-doped graphene sheets by a combined chemical and hydrothermal reduction of graphene oxide. *Langmuir* **2010**, *26*, 16096–16102. [CrossRef] [PubMed]
52. Robinson, M.; Hensley, J.E.; Medlin, J.W. Bifunctional Catalysts for Upgrading of Biomass-Derived Oxygenates: A Review. *ACS Catal.* **2016**, *6*, 5026–5043. [CrossRef]
53. Pang, J.; Sun, J.; Zheng, M.; Li, H.; Wang, Y.; Zhang, T. Transition metal carbide catalysts for biomass conversion: A review. *Appl. Catal. B Environ.* **2019**, *254*, 510–522. [CrossRef]
54. Zhang, J.; Zhang, M.; Zeng, Y.; Chen, J.; Qiu, L.; Zhou, H.; Sun, C.; Yu, Y.; Zhu, C.; Zhu, Z. Single Fe atom on hierarchically porous S, N-codoped nanocarbon derived from porphyra enable boosted oxygen catalysis for rechargeable Zn-air batteries. *Small* **2019**, *15*, 1900307. [CrossRef]
55. Zhu, M.; Xie, P.; Fan, L.F.; Rong, M.Z.; Zhang, M.Q.; Zhang, Z.P. Performance improvement of N-doped carbon ORR catalyst via large through-hole structure. *Nanotechnology* **2020**, *31*, 335717. [CrossRef]
56. Sullivan, M.M.; Bhan, A. Acetone hydrodeoxygenation over bifunctional metallic−Acidic molybdenum carbide Catalysts. *ACS Catal.* **2016**, *6*, 1145–1152. [CrossRef]
57. Xu, G.Y.; Guo, J.H.; Qu, Y.C.; Zhang, Y.; Fu, Y.; Guo, Q.X. Selective hydrodeoxygenation of lignin-derived phenols to alkyl cyclohexanols over a Ru-solid base bifunctional catalyst. *Green Chem.* **2016**, *18*, 5510. [CrossRef]
58. Ishikawa, M.; Tamura, M.; Nakagawa, Y.; Tomishige, K. Demethoxylation of guaiacol and methoxybenzenes over carbon-supported Ru–Mn catalyst. *Appl. Catal. B* **2016**, *182*, 193–203. [CrossRef]
59. Chieffi, G.; Giordano, C.; Antonietti, M.; Esposito, D. FeNi nanoparticles with carbon armor as sustainable hydrogenation catalysts: Towards biorefineries. *J. Mater. Chem. A* **2014**, *2*, 11591–11596. [CrossRef]
60. Kim, S.; Tsang, Y.F.; Kwon, E.E.; Lin, K.Y.A.; Lee, J. Recently developed methods to enhance stability of heterogeneous catalysts for conversion of biomass-derived feedstocks. *Korean J. Chem. Eng.* **2019**, *36*, 1–11. [CrossRef]
61. Wu, S.K.; Lai, P.C.; Lin, Y.C.; Wan, H.P.; Lee, H.T.; Chang, Y.H. Atmospheric Hydrodeoxygenation of guaiacol over alumina-, zirconia-, and silica-supported nickel phosphide catalysts. *ACS Sustain. Chem. Eng.* **2013**, *1*, 349–358. [CrossRef]
62. Lan, X.; Hensen, E.J.M.; Weber, T. Hydrodeoxygenation of guaiacol over Ni_2P/SiO_2–reaction mechanism and catalyst deactivation. *Appl. Catal. A–Gen.* **2018**, *550*, 57–66. [CrossRef]
63. Schutyser, W.; Van den Bosch, S.; Dijkmans, J.; Turner, S.; Meledina, M.; Tendeloo, G.V.; Debecker, D.P.; Sels, B.F. Selective Nickel-Catalyzed Conversion of Model and Lignin-Derived Phenolic Compounds to Cyclohexanone-Based Polymer Building Blocks. *ChemSusChem* **2015**, *8*, 1805–1818. [CrossRef] [PubMed]